Spacecraft Dynamics Under the Action of Y-dot Magnetic Control Law

Alessandro Zavoli[a,1,*], Fabrizio Giulietti[b,2], Giulio Avanzini[c,3], Guido De Matteis[a,4]

[a]*'Sapienza' Università di Roma, Rome, Italy 00184*
[b]*Università di Bologna, Forlì, Italy 47121*
[c]*Università del Salento, Lecce, Italy 73100*

Abstract

The paper investigates the dynamic behavior of a spacecraft when a single magnetic torque-rod is used for achieving a pure spin condition by means of the so-called Y-dot control law. Global asymptotic convergence to a pure spin condition is proven on analytical grounds when the dipole moment is proportional to the rate of variation of the component of the magnetic field along the desired spin axis. Convergence of the spin axis towards the orbit normal is then explained by estimating the average magnetic control torque over one orbit. The validity of the analytical results, based on some simplifying assumptions and approximations, is finally investigated by means of numerical simulation for a fully nonlinear attitude dynamic model, featuring a tilted dipole model for Earth's magnetic field. The analysis aims to support, in the framework of a sound mathematical basis, the development of effective control laws in realistic mission scenarios. Results are presented and discussed for relevant test cases.

Keywords: spacecraft control, underactuated systems, magnetic control, nonlinear systems

1. Introduction

This paper deals with magnetic control of small spacecraft based on the so-called Y-dot control law. The case of spacecraft with arbitrary inertia tensor using a single magnetic torque-rod for detumbling is considered and the analysis is focused on the property of generalized exponential asymptotic stability in variations (GEASV) of the pure-spin equilibrium points. Also, the mechanism of the alignment of the spin axis to the orbit normal in a general geomagnetic field is explained in physical terms, and proved analytically. As a further contribution, a comprehensive numerical study is performed in order to evaluate the relationship between the value of the (uncontrolled) final pure-spin rate, on one side, and spacecraft initial rotational energy and inertia tensor on the other one.

In the framework of small satellite, magnetic control has been increasingly gaining in popularity. Ease of design, absence of moving parts, low mass, and need for renewable-only electrical power to operate make magnetic actuator quite appealing for space applications (especially for low Earth orbit missions where the magnitude of the magnetic field is stronger). As a drawback, magnetic-only controlled system are inherently underactuated, as no torque can be produced along the direction of the instantaneous local magnetic field vector. In this respect, practical control solutions exploit the variability of the geomagnetic field as sensed by the spacecraft, which primarily depends on spacecraft attitude dynamics and orbital motion. Magnetic control proved to be a viable solution for a variety of mission tasks, spanning from (coarse) full attitude stabilization [1, 2], reaction or momentum bias wheels desaturation [3], to initial detumbling after spacecraft separation [4]. The latter application is considered in the present study.

---

*Corresponding author. Tel.: +39 06 44585786; E-mail address: alessandro.zavoli@uniroma1.it
[1]Research Assistant, Department of Mechanical and Aerospace Engineering
[2]Associate professor, Department of Industrial Engineering (DIN)
[3]Professor, Department of Engineering
[4]Professor, Department of Mechanical and Aerospace Engineering

The detumbling phase is crucial for small spacecraft, which are often launched as a secondary payload (aside a more important/expensive payload) and released at an unknown, and often high, tumbling rate. A reliable, rapid, and cost-effective reduction of the angular rate below a given threshold is commonly required prior to the deployment of solar arrays, when present, as well as any other mission-related task (such as Sun acquisition, initial attitude determination, Earth pointing, etc.).

Magnetic detumbling of a spacecraft may be attained by means of simple command laws such as the B-dot controller [4]. The B-dot command law allows one to drive the initial angular velocity to (almost) zero, without requiring attitude or rate information. Only measurements of the Earth magnetic field are required. Theoretical [5] and practical [6] aspects of this controller has been extensively studied, proving the viability of the approach and estimating its expected performance.

Several variants of the B-dot controller have been proposed over the last few years. Many of them aim to drive the spacecraft towards a non-zero angular velocity, where a final spinning condition allows one to reduce thermal loads, by avoiding prolonged exposition of the Sun-facing side to solar radiation. In other cases, a residual spinning motion is required to preserve a certain amount of angular momentum necessary to spin up the momentum wheel that provides gyroscopic stabilization [7].

In the present paper, a single-axis B-dot control law, also known as β-dot or Y-dot command law (due to the fact that the pitch, y, axis is the most common choice as commanded axis) is considered. By using a single magnetic torque-rod this controller (usually adopted in conjunction to a spin-rate controller, which makes use of an additional orthogonally-placed magnetic torque-rod) can reduce the initial tumbling rate, eventually steering the satellite either towards a pure spin condition around one of its principal axes of inertia or to an almost zero residual angular rate. Its effectiveness was demonstrated through simulations before being successfully applied in several missions, such as SNAP-1 [8], FalconSAT-3 [9], UoSAT-12 [10], Alsat-1 [11], and SUMBANDILASAT [12].

Despite the conceptual simplicity of a Y-dot controller, a rigorous analysis of closed-loop system dynamics, characterizing the properties of the resulting motion (e.g. global asymptotic convergence towards a terminal pure-spin condition, spin-axis direction with respect to the orbit frame, etc.), is far from trivial. Nevertheless, such an analysis is necessary for supporting a mathematically sound approach to the synthesis of a control system which guarantees adequate performance in an realistic mission scenario.

This subject was recently investigated in [13], where the actions of both B-dot and Y-dot controllers were considered within a simplified, "circular", geomagnetic field model. Under the assumptions that (i) magnetic induction vector describes a circular cone in the orbit frame (rather than an elliptical one, as it results from the widely used tilted dipole model [14]), and (ii) the spacecraft is an axi-symmetric rigid body, an averaging technique allowed for an elegant analytical derivation of relevant controller properties. A further numerical analysis, which retains the same simplifying assumptions on the geomagnetic field, was presented in [15].

The present paper aims at generalizing these results, by proving global asymptotic convergence to a pure spin state for the Y-dot control law even in the case of a tri-inertial spacecraft and without further assumptions on the geomagnetic field model. A variational system approach [16] to the stability analysis of nonlinear systems is pursued. The equations of motion for system dynamics are recast in the form of a nominal system perturbed by a vanishing perturbation term. Global exponential asymptotic stability (EAS) of the origin for the nominal system is proven first. Robustness of the stability of the nominal system is then invoked in order to derive generalized exponential asymptotic stability in variations (GEASV) of the perturbed system [17]. The inertial position of the spin axis is also considered, proving that, under the assumptions valid for a tilted-dipole geomagnetic field model, the Y-dot control law eventually aligns the spin axis with the direction normal to the orbit plane, regardless of the initial condition. The convergence of the spin axis towards the orbit normal is proven by estimating the average magnetic control torque over one orbit.

The study is completed by a detailed numerical analysis of the spacecraft pure-spin final state as a function of the initial tumbling motion and spacecraft mass distribution, assuming that no control is performed other than the Y-dot (i.e., using only one magnetic torque-rod). In particular, the relationship between final pitch rate, initial spacecraft rotational energy, and spacecraft inertia matrix is analyzed, identifying those conditions that may lead to a complete detumbling of the spacecraft, which is quite a relevant feature for the

practical application of this command law. An insightful explanation is proposed in terms of polhode curves and energy-dissipation. It is also proven that the adopted control law aligns spacecraft angular velocity vector to the direction opposite to the orbit angular rate, so that the pitch axis becomes parallel to the orbit normal, for a positive asymptotic value of the pitch rate, or points in the opposite direction, for a negative pitch rate.

The article is organized as follows: a quick outline of system dynamics and of the Y-dot control law is provided in Section 2. After a review of a few relevant nonlinear system stability theorems, a proof for the stability of the pure spin condition around the pitch axis is given in Section 3. The validity of the results, together with expected performance from the control approach are extensively tested and discussed by means of numerical simulation, discussed in Section 4. A section of conclusions ends the paper.

2. Problem Statement

2.1. System dynamics

Spacecraft dynamics, expressed in terms of angular momentum in a set of principal axes of inertia, $\mathbb{F}_B = \{P; \hat{\boldsymbol{e}}_1, \hat{\boldsymbol{e}}_2, \hat{\boldsymbol{e}}_3\}$, centered in the spacecraft center of mass P, is described by the equation

$$\boldsymbol{I}\,\dot{\boldsymbol{\omega}} = \boldsymbol{M} - \boldsymbol{\omega} \times \boldsymbol{I}\,\boldsymbol{\omega} \tag{1}$$

where $\boldsymbol{\omega} = (\omega_1, \omega_2, \omega_3)^T$ is the absolute angular velocity vector, and $\boldsymbol{I} = \mathrm{diag}(J_1, J_2, J_3)$ is the spacecraft inertia matrix.

An orbital reference frame, $\mathbb{F}_O = \{P; \hat{\boldsymbol{o}}_1, \hat{\boldsymbol{o}}_2, \hat{\boldsymbol{o}}_3\}$, is also introduced, centered in the spacecraft center of mass P, such that the $\hat{\boldsymbol{o}}_3$ unit vector lies along the local vertical, towards the center of the Earth, the $\hat{\boldsymbol{o}}_2$ unit vector is normal to the orbit plane, in a direction opposite to the orbital angular speed $\boldsymbol{\omega}^{orb}$, and the transverse axis $\hat{\boldsymbol{o}}_1$ completes a right-handed triad, in the direction of the orbital velocity, when the orbit is circular. A circular low Earth orbit of radius r_c, period T_{orb}, and orbit rate $\Omega = \|\boldsymbol{\omega}^{orb}\| = 2\pi/T_{orb}$ is considered. Satellite attitude with respect to the orbit frame $\mathbb{F}_O$ is represented by means of a unit quaternion $\boldsymbol{Q} = (\boldsymbol{q}^T, \bar{q})^T$ [18], which evolves as a function of the relative angular speed $\boldsymbol{\omega}^r = \boldsymbol{\omega} - \mathbb{T}_{BO}\,\boldsymbol{\omega}_O^{orb}$, where $\boldsymbol{\omega}_O^{orb} = (0, -\Omega, 0)^T$ is the angular speed of $\mathbb{F}_O$ with respect to an inertial frame and $\mathbb{T}_{BO}$ is the coordinate transformation matrix between $\mathbb{F}_O$ and $\mathbb{F}_B$. The geometry of the problem is sketched in Fig. 1.
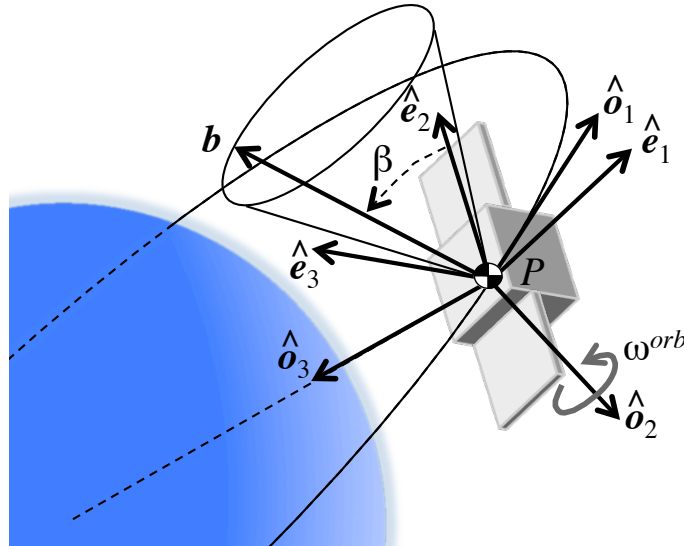

Figure 1: Geometry of the problem.

No external disturbance is considered in the analysis, so that the only external torque acting on the spacecraft is the magnetic control torque, $\boldsymbol{M} = \boldsymbol{m} \times \boldsymbol{b}$, where $\boldsymbol{m}$ is the magnetic dipole moment vector generated by the coils, $\boldsymbol{b} = \mathbb{T}_{BO} \, \boldsymbol{b}_O$ is the local geomagnetic field vector expressed in terms of body-frame components, $\boldsymbol{b}_O$ is the geomagnetic field vector expressed in the orbit frame. For a circular orbit, Earth geomagnetic field can be approximated by a tilted magnetic dipole of moment $M_\oplus = 7.8379 \times 10^6$ T km^3, with a tilt angle $\gamma_m = 11.44$ deg with respect to the polar axis [14]. Its components can be expressed in $\mathbb{F}_O$ as in [3]:

$$\boldsymbol{b}_O = \frac{M_\oplus}{r_c^3} \begin{bmatrix} \sin \xi_m \, \cos(\Omega\, t - \eta_m) \\ -\cos \xi_m \\ 2 \, \sin \xi_m \, \sin(\Omega\, t - \eta_m) \end{bmatrix} \tag{2}$$

where

$$\cos \xi_m = \cos i \, \cos \gamma_m + \sin i \, \sin \gamma_m \, \cos \beta'_m$$

$$\sin \eta_m \, \sin \xi_m = -\sin \gamma_m \, \sin \beta'_m$$

$$\cos \eta_m \, \sin \xi_m = \sin i \, \cos \gamma_m - \cos i \, \sin \gamma_m \, \cos \beta'_m$$

$$\beta'_m = \beta_m + \omega_e \, t - \Omega_{an}$$

In these equations, i is the orbit inclination, Ω is the orbit rate, ω_e is the Earth spin rate around its polar axis, Ω_{an} is the ascending node of the spacecraft orbit, and β_m is the initial value of the angle between the vernal equinox and the line of intersection of the equatorial plane with the geomagnetic equator. The angle ξ_m represents the inclination of spacecraft orbit relative to the geomagnetic equatorial plane, and η_m is the angle between the ascending node relative to the Earth's equator and the ascending node relative to the geomagnetic equator.

2.2. The Y-dot control law

As anticipated in the previous section, the Y-dot control law is obtained as a reduced (single-axis) version of the B-dot control law, that is, by activating only the magnetic coil aligned with the pitch axis and commanding a dipole moment proportional to the time derivative of the pitch component of the magnetic field sensed in the body reference frame. Therefore, the control dipole moment is given by

$$\boldsymbol{m} = -k_y \dot{b}_2 \hat{\boldsymbol{e}}_2 \tag{3}$$

where k_y is a control gain and $\hat{\boldsymbol{e}}_2$ is the unit vector aligned to the pitch axis.

A variant of the considered command law, named β-dot, is proposed in [10], where the dipole moment is proportional to the rate of variation of the angle between the direction of the magnetic field and that of the pitch axis, $\beta = \cos^{-1}(b_2/\|\boldsymbol{b}\|)$. The magnetic dipole moment in this case is equal to

$$\boldsymbol{m} = k_\beta \dot{\beta} \hat{\boldsymbol{e}}_2 \tag{4}$$

However, the use of an inverse cosine function poses an obstacle for the derivation of a formal proof of stability, provided that the expression of $\dot{\beta}$ becomes singular when $\beta \to 0, \pi$. For this reason, in what follows, only the formulation of the Y-dot control law expressed in Eq. (3) will be considered.

3. Convergence/Stability analysis of the Y-dot control law

3.1. Relevant results from nonlinear control theory

This section recalls some useful results from nonlinear system theory, with particular attention on definitions and theorems from the method of variational system for the analysis of stability of nonlinear non-autonomous system [19, 20].

Consider the nonlinear differential system $\dot{\boldsymbol{x}} = \boldsymbol{f}(t, \boldsymbol{x})$, with $\boldsymbol{x}(0) = \boldsymbol{x}_0$. Let $\boldsymbol{\Phi}(t, t_0, \boldsymbol{x}_0) = \partial\, \boldsymbol{x}(t, t_0, \boldsymbol{x}_0)/\partial\, \boldsymbol{x}_0$ be the fundamental matrix, solution of the variational system $\dot{\boldsymbol{z}} = \boldsymbol{f}_x(t, t_0, x_0)\boldsymbol{z}$, which is the identity matrix for $t = t_0$, such that $\boldsymbol{x}(t, t_0, \boldsymbol{x}_0) = \boldsymbol{\Phi}(t, t_0, \boldsymbol{x}_0)\boldsymbol{x}_0$. The following stability definitions are introduced

Definition 1 *The solution $\boldsymbol{x} = \boldsymbol{0}$ of the system $\dot{\boldsymbol{x}} = \boldsymbol{f}(t, \boldsymbol{x})$ is said to be*

1. *exponentially asymptotically stable (EAS) if there exist constants $K > 0$, $c > 0$ such that*

$$\|\boldsymbol{x}(t, t_0, \boldsymbol{x}_0)\| \leq K \|\boldsymbol{x}_0\| e^{-c(t-t_0)} \tag{5}$$

2. *uniformly stable in variation if there exists a constant M such that*

$$\|\boldsymbol{\Phi}(t, t_0, \boldsymbol{x}_0)\| \leq M \qquad \forall t > t_0, \ and \ \|\boldsymbol{x}_0\| < \infty \tag{6}$$

3. *exponentially stable in variation if there exist two constants $K > 0$, $\alpha > 0$ such that*

$$\|\boldsymbol{\Phi}(t, t_0, \boldsymbol{x}_0)\| \leq K e^{-\alpha t} \qquad \forall t \geq t_0 \geq 0, \ and \ \|\boldsymbol{x}_0\| < \infty \tag{7}$$

4. *generalized exponentially asymptotically stable in variation (GEASV) if*

$$\|\boldsymbol{\Phi}(t, t_0, \boldsymbol{x}_0)\| \leq K(t) \, e^{\, p(t_0) - p(t)} \qquad \forall t \geq t_0 \geq 0, \ and \ \|\boldsymbol{x}_0\| < \infty \tag{8}$$

where $K > 0$ is continuous on $\mathbb{R}^+$, and $p \in C(\mathbb{R}^+)$, $p(0) = 0$, is strictly increasing in $t \in \mathbb{R}^+$.

If the constants do not depend on the initial condition, $\boldsymbol{x}_0$, the stability property is said to be global.

As the reader may notice, the stability in variation is defined over the norm of the fundamental matrix $\boldsymbol{\Phi}(t, t_0, x_0)$, with the corresponding (Lyapunov) stability being defined over the norm of the solution, or more precisely on the ratio $\|\boldsymbol{x}(t, t_0, x_0)\| / \|\boldsymbol{x}_0\|$. The stability in variation of an equilibrium point always implies the corresponding (Lyapunov) stability, e.g., asymptotic stability in variation (ASV) implies asymptotic stability (AS), and so on. The converse implication is, in general, false. As a result, the condition of stability in variation appears somehow stronger than the corresponding (Lyapunov) stability. Implications across different types of stability are well documented in [19]. Indeed, for linear systems, the two definitions of stability and stability in variations coincide. A relevant, non-trivial, case is represented by the equivalence between EASV and EAS for linear time-varying systems, which is proven in Theorem 4.11 of [21].

Two theorems invoked in the derivation of the stability proof of the Y-dot control law are recalled below.

Theorem 1 *Given the linear time-varying perturbed system $\dot{\boldsymbol{x}} = \boldsymbol{A}(t)\,\boldsymbol{x} + \boldsymbol{g}(t, \boldsymbol{x})$, let the origin $\boldsymbol{x} = \boldsymbol{0}$ be an exponentially stable solution of the nominal system $\dot{\boldsymbol{x}} = \boldsymbol{A}(t)\,\boldsymbol{x}$, and the perturbed term satisfies the inequality $\|\boldsymbol{g}(t, \boldsymbol{x})\| \leq \bar{\varphi} \|\boldsymbol{x}\|$, $\bar{\varphi} > 0$, $t \geq t_0 \geq 0$, $\|\boldsymbol{x}\| < \infty$. Then every solution of the perturbed system is GEASV.*

Theorem 2 *Consider a nonlinear non-autonomous dynamic system $\dot{\boldsymbol{x}} = \boldsymbol{f}(t, \boldsymbol{x})$, where $\boldsymbol{f} : \mathbb{R}^n \times \mathbb{R} \to \mathbb{R}^n$ is piecewise continuous in t and Lipschitz in $\boldsymbol{x}$. Let $\boldsymbol{x} = \boldsymbol{0}$ be an equilibrium point for the system at $t = 0$. Also assume that a strictly positive definite Lyapunov-like function $V(\boldsymbol{x}) > 0$ exists, where (i) $V : \mathbb{R}^n \to \mathbb{R}$ is a smooth scalar function of the state $\boldsymbol{x}$ only and (ii) its gradient vanishes at the origin only, that is, $\nabla_x V = \boldsymbol{0}$ at $\boldsymbol{x} = \boldsymbol{0}$ and $\nabla_x V \neq \boldsymbol{0}$ elsewhere. If the Lyapunov-like function $V(\boldsymbol{x})$ and its time derivative $\dot{V}(t, \boldsymbol{x})$ satisfy the conditions:*

1. *$k_1 \|\boldsymbol{x}\|^c \leq V(\boldsymbol{x}) \leq k_2 \|\boldsymbol{x}\|^c$ $k_1 > 0, k_2 > 0, c > 0$;*
2. *$\dot{V}$ is negative semi-definite, that is, $\dot{V}(t, \boldsymbol{x}) \leq 0$;*
3. *$\dot{V}$ is uniformly continuous;*
4. *the iso-surfaces S of $V(\boldsymbol{x})$ in the state space $\mathbb{R}^n$ do not contain any integral curves $\boldsymbol{x}(t)$ of the vector field $\boldsymbol{f}$ other than the constant ones ($\boldsymbol{x}(t) = \boldsymbol{x}_e, \forall t$);*

then the state converges to one of the (at least locally) stable equilibria. If the origin is the only equilibrium, it is globally exponentially stable.

These theorems, proven in [7], stem from the nonlinear system dynamics theory and are of general validity. They are here recalled as their application to the problem under investigation is straightforward. More specifically, Theorem 1 provides conditions such that GEASV of a linear time-varying perturbed system is guaranteed if the origin of the nominal system is globally exponentially asymptotically stable. In its proof use is made of the linearity of the nominal system to demonstrate that it is GEASV. Theorem 3.8 from [17] concerning the robustness of the generalized exponential stability in variation of the nominal system under vanishing perturbation is then applied. At the same time, Theorem 2 poses conditions for global exponential stability of the origin for a specific class of nonlinear, non-autonomous systems. Its proof was derived by applying Theorem 8.5 from [21].

3.2. Acquisition of a pure spin condition around the pitch axis

The purpose of this section is to prove that the Y-dot control law, Eq. (3), drives the spacecraft towards a terminal condition of pure-spin about the pitch axis, that is, the final angular velocity matches the form $\boldsymbol{\omega} = (0, \omega_2, 0)$, for some constant $\omega_2 \in \mathbb{R}$, which depends on initial conditions.

During the initial phase of the detumbling maneuver it is possible to assume $\|\boldsymbol{\omega}\| \gg \Omega$, and $\dot{\boldsymbol{b}} \approx -\boldsymbol{\omega} \times \boldsymbol{b}$. This implies that the second component of $\dot{\boldsymbol{b}}$ in Eq. (3) can be expressed as $\dot{b}_2 \approx b_3 \omega_1 - b_1 \omega_3$.

Consequently the command torque $\boldsymbol{M} = \boldsymbol{m} \times \boldsymbol{b}$ is given by

$$\boldsymbol{M} = -k_y \begin{bmatrix} b_3^2 & 0 & -b_1 b_3 \\ 0 & 0 & 0 \\ -b_1 b_3 & 0 & b_1^2 \end{bmatrix} \begin{pmatrix} \omega_1 \\ \omega_2 \\ \omega_3 \end{pmatrix} \tag{9}$$

Obviously, no torque is produced along the body pitch (y) axis $\hat{\boldsymbol{e}}_2$.

In order to prove that first and third components of the angular velocity tend to vanish under the Y-dot control law, let us study the stability of the origin of the reduced dynamic system obtained by selecting the first and third rows of the full spacecraft attitude dynamics. By applying a selection matrix $\boldsymbol{S} = \begin{bmatrix} \hat{\boldsymbol{e}}_1 & \hat{\boldsymbol{e}}_3 \end{bmatrix}^T$ to Eq. (1), one obtains

$$\boldsymbol{I}_{13} \dot{\boldsymbol{\omega}}^\star = -k_y \boldsymbol{P}^\star(t) \boldsymbol{\omega}^\star - \boldsymbol{S}[\boldsymbol{\omega} \times (\boldsymbol{I}\boldsymbol{\omega})] \tag{10}$$

where $\boldsymbol{\omega}^\star = (\omega_1, \omega_3)^T$ is the vector containing the roll (x) and yaw (z) angular rates, and the reduced torque is defined as $\boldsymbol{M}^\star = \boldsymbol{S}\boldsymbol{M} = -k_y \boldsymbol{P}^\star \boldsymbol{\omega}^\star$, with

$$\boldsymbol{P}^\star(t) = \begin{bmatrix} b_3^2 & -b_1 b_3 \\ -b_1 b_3 & b_1^2 \end{bmatrix} \tag{11}$$

The system in the form of Eq. (10) matches the classical linear time-varying perturbed system structure required by Theorem 1, namely

$$\dot{\boldsymbol{\omega}}^\star = \boldsymbol{A}(t) \boldsymbol{\omega}^\star + \boldsymbol{g}(t, \boldsymbol{\omega}^\star) \tag{12}$$

where the time-varying matrix

$$\boldsymbol{A}(t) = -k_y \boldsymbol{I}_{13}^{-1} \boldsymbol{P}^\star(t) = -k_y \boldsymbol{I}_{13}^{-1} \begin{bmatrix} b_3^2 & -b_1 b_3 \\ -b_1 b_3 & b_1^2 \end{bmatrix} \tag{13}$$

governs the nominal system, and

$$\boldsymbol{g}(t, \boldsymbol{\omega}^\star) = -\boldsymbol{I}_{13}^{-1} \boldsymbol{S}[\boldsymbol{\omega} \times (\boldsymbol{I}\boldsymbol{\omega})] = \omega_2 \begin{bmatrix} 0 & (J_3 - J_2) \\ (J_1 - J_2) & 0 \end{bmatrix} \begin{pmatrix} \omega_1 \\ \omega_3 \end{pmatrix} \tag{14}$$

is a vanishing perturbation term.

Global exponential stability of the origin $\boldsymbol{\omega}^\star = \boldsymbol{0}$ for the nominal system

$$\dot{\boldsymbol{\omega}}^\star = \boldsymbol{A}(t) \boldsymbol{\omega}^\star \tag{15}$$

6

can be proved by means of Theorem 2. In particular, the Lyapunov candidate function V

$$V(\boldsymbol{\omega}^\star) = 1/2\,\boldsymbol{\omega}^{\star\,T}\boldsymbol{I}_{13}\,\boldsymbol{\omega}^\star \tag{16}$$

with time derivative $\dot{V}$

$$\dot{V}(\boldsymbol{\omega}^\star) = -k_y\boldsymbol{\omega}^{\star\,T}\boldsymbol{P}^\star(t)\boldsymbol{\omega}^\star \tag{17}$$

clearly satisfies Conditions 1, 2, and 3 of the Theorem.

Condition 4 requires that the iso-surfaces S of $V(\boldsymbol{\omega}^\star) = (1/2)(J_1\omega_1^2 + J_3\omega_3^2) = C$, with $C > 0$ a positive constant, do not contain solutions $\boldsymbol{\omega}^\star(t)$ of Eq. (15), other than constant ones. This can be proven by noting that, taking the time derivative of V, one gets $\dot{V} = J_1\omega_1\dot{\omega}_1 + J_3\omega_3\dot{\omega}_3 = 0$. Upon substitution of the expressions of the components of $\dot{\boldsymbol{\omega}}^\star$ from Eq. (15), the equation $\dot{V} = 0$ holds if

$$k_y(b_3\omega_1 - b_1\omega_3)^2 = 0 \tag{18}$$

that is, if $\boldsymbol{\omega}^\star(t) = \Omega^\star(t)\,\boldsymbol{Sb}(t) = \Omega^\star(t)\,(b_1(t), b_3(t))^T$, with $\Omega^\star(t) = \|\boldsymbol{\omega}^\star(t)\|$. If this tentative solution is substituted in Eq. (15), one gets $\dot{\omega}_1 = \dot{\omega}_3 = 0$, that is, only constant solutions for the state vector of the nominal system are expected, and Condition 4 is satisfied.

For proving global exponential stability, it is also necessary to show that the origin is the only admissible equilibrium for Eq. (15), when the variation of the elements of $\boldsymbol{A}(t)$ follows a physically admissible pattern. Beside the origin $\boldsymbol{\omega}^\star = (0, 0)$, which is a fixed point for any value of $b_1(t)$ and $b_3(t)$, the nominal LTV system represented by Eq. (15) has two more equilibria:

(a) $\boldsymbol{\omega}^\star = (\tilde{\omega}_1, 0)$ if $b_3(t) \equiv 0$, for any value of $b_1(t)$ and $\tilde{\omega}_1 \in \mathbb{R}$

(b) $\boldsymbol{\omega}^\star = (0, \tilde{\omega}_3)$ if $b_1(t) \equiv 0$, for any value of $b_3(t)$ and $\tilde{\omega}_3 \in \mathbb{R}$

It is possible to show that neither of them is physically admissible. The equilibrium (a) is discussed, but the same argument applies to (b). The equilibrium (a) refers to the cases of a satellite in a pure spin motion about axis $\hat{\boldsymbol{e}}_1$, which is parallel to the magnetic field vector $\boldsymbol{b}$. In this circumstance, the angular velocity component ω_3 and the component b_3 of the geomagnetic vector in $\mathbb{F}_B$ should simultaneously remain identically zero over time. However, due to the orbital motion, the direction of the geomagnetic field acting on the spacecraft changes with time, whereas the angular velocity vector (which in case of pure spin motion is parallel to the angular momentum) is inertially fixed. Consequently, the condition for the existence of equilibrium (a) or (b) cannot be maintained. This implies that the origin $\boldsymbol{\omega}^\star = (0, 0)$ is the only physically admissible equilibrium for Eq. (15), and by means of Theorem 2 global exponential stability is proven.

One can easily show that the perturbation term of Eq. (12), written in Eq. (14), satisfies the condition $\|\boldsymbol{g}(t, \boldsymbol{\omega}^\star)\| \le \bar{\varphi}\,\|\boldsymbol{\omega}^\star\|$, $t \ge t_0 \ge 0$, $\|\boldsymbol{\omega}^\star\| < \infty$ of Theorem 1. The last inequality holds if one chooses

$$\bar{\varphi} = \sqrt{(2\mathcal{T}_0/J_2)\,|\,(J_3 - J_2)\,(J_2 - J_1)\,|} \tag{19}$$

where $\mathcal{T}_0$ is the initial rotational kinetic energy

First, note that the ω_2 angular rate remains bounded during the maneuver: the rotational kinetic energy $\mathcal{T} = (1/2)\boldsymbol{\omega}^T\boldsymbol{I}\boldsymbol{\omega}$ is a non-increasing quantity under the action of the Y-dot control law, with its time derivative

$$\dot{\mathcal{T}} = \boldsymbol{\omega}^T\boldsymbol{M} = -k_y\boldsymbol{\omega}^T \begin{bmatrix} b_3^2 & 0 & -b_1 b_3 \\ 0 & 0 & 0 \\ -b_1 b_3 & 0 & b_1^2 \end{bmatrix} \boldsymbol{\omega} \tag{20}$$

being a semi-definite negative quadratic form. Therefore, the maximum absolute value of ω_2 is bounded by the value corresponding to a pure spin rotation about the y axis, evaluated for the initial rotational energy, that is, $\|\omega_2\| \le \sqrt{2\mathcal{T}_0/J_2}$. Moreover, the matrix between square brackets in Eq. (14) is a constant term,

with spectral norm equal to $(|\,(J_3 - J_2)\,(J_2 - J_1)\,|)^{1/2}$. Thus, as all hypoteses of Theorem 1 are verified, the equilibrium point $\boldsymbol{\omega}^{\star} = \boldsymbol{0}$ is proven to be GEASV.

Remark 1: The previous demonstration proves the stability of the origin for the reduced angular rate in the $\{\omega_1, \omega_3\}$ space. In the ω_2 subspace, the solution is only locally stable, as confirmed by an elementary linear stability analysis.

Remark 2: The command law, as expressed in Eq. (3), will cause the spacecraft to converge towards a pure spin condition around the pitch axis, where the asymptotic value of ω_2 can be different from zero. In this case the residual kinetic energy is entirely transferred to the pitch axis. The value of the spin rate at convergence is not controlled and, in general, the result discussed above also allows for a complete detumbling, in those cases when the entire initial kinetic energy is dissipated and, as a consequence, also ω_2 converges to zero.

Remark 3: Provided that the presence of time-varying roll and yaw rates induces dissipation, which in turn reduces the final pitch rate, when present, it is possible to deduce that, in those cases when the control axis is not a principal axis of inertia the condition $\boldsymbol{\omega} = (0, \omega_2, 0)$ is not an equilibrium point. The gyroscopic coupling term remains non-zero, thus preventing the spacecraft from reaching a pure spin condition around the y axis. In case of a minor misalignment between the control axis and a principal axis of inertia, the final spin rate is expected to become significantly small in the long run, and possibly to completely vanish when the misalignment becomes more significant, and the corresponding cross-coupling term more severe.

3.3. Spin axis alignment with orbit normal

Once a pure spin condition around the y-axis is obtained, the angular velocity vector, $\boldsymbol{\omega}$, and the angular momentum vector, $\boldsymbol{h}$, are parallel to the desired spin axis, $\hat{\boldsymbol{e}}_2$, which points along an inertially fixed direction, in the absence of external torques. In general, this direction forms an angle γ with the direction normal to the orbit plane, $\hat{\boldsymbol{o}}_2$. When the Y-dot control law is maintained active after the pure spin condition around $\hat{\boldsymbol{e}}_2$ is achieved, the angle γ slowly decreases, until the spin axis becomes parallel to $\hat{\boldsymbol{o}}_2$. This long-term effect, already observed in [8] and [9], can be explained as follows.

Assume that $\hat{\boldsymbol{e}}_2^0$ is the direction of the spin axis at a given time instant t_0, after the pure spin condition is acquired. It is possible to define an inertially fixed auxiliary frame $\mathbb{F}_O^* = \{P; \hat{\boldsymbol{o}}_1^*, \hat{\boldsymbol{o}}_2, \hat{\boldsymbol{o}}_3^*\}$, where $\hat{\boldsymbol{o}}_3^* = \hat{\boldsymbol{e}}_2^0 \times \hat{\boldsymbol{o}}_2 / \|\hat{\boldsymbol{e}}_2^0 \times \hat{\boldsymbol{o}}_2\|$ and $\hat{\boldsymbol{o}}_1 = \hat{\boldsymbol{o}}_2 \times \hat{\boldsymbol{o}}_3$ completes a right-handed triad (Fig. 2). Note that $\hat{\boldsymbol{o}}_1^*$ is directed as the projection of $\hat{\boldsymbol{e}}_2^0$ on the orbit plane.

Following the notation introduced in Fig. 2, the components of the spin axis and of the geomagnetic vector in $\mathbb{F}_O^*$ are given by

$$\hat{\boldsymbol{e}}_2 = (\sin \gamma \cos \tau, -\cos \gamma, \sin \gamma \sin \tau)^T \tag{21}$$

$$\boldsymbol{b} = \|\boldsymbol{b}\|(\sin \delta \cos \sigma, -\cos \delta, \sin \delta \sin \sigma)^T \tag{22}$$

where γ, τ are spherical coordinates used to express $\hat{\boldsymbol{e}}_2$ components in the orbital frame $\mathbb{F}_O$ and $\|\boldsymbol{b}\|$ is the intensity of the geomagnetic field. The unit vector $\hat{\boldsymbol{b}}$ rotates around the orbit normal during one revolution. The angle σ thus undergoes a variation of 4π over one orbit, in the inertially fixed frame $\mathbb{F}_O^*$, whereas the variation of δ remains bounded, when $\boldsymbol{b}$ follows the surface of an elliptical cone, as described by the geomagnetic model of Eq. (2). Provided that in this phase the magnetic torque delivered by the Y-dot control law is small, it is possible to assume that the variation of the direction of the angular momentum vector $\boldsymbol{h}$, which is almost exactly parallel to $\hat{\boldsymbol{e}}_2$, is slow. Over one orbit after t_0, the angle τ remains close to zero, and

$$\hat{\boldsymbol{e}}_2 \approx (\sin \gamma, -\cos \gamma, 0)^T \tag{23}$$

The magnetic dipole moment is proportional to the time derivative of $\hat{b}_2$, where $\hat{b}_2 = \hat{\boldsymbol{b}}^T \hat{\boldsymbol{e}}_2 = \sin \delta \cos \sigma \sin \gamma + \cos \delta \cos \gamma$. If $\dot{\gamma}, \dot{\delta} \ll \dot{\sigma} = \mathcal{O}(2\Omega)$, it is possible to approximate $\dot{\hat{b}}_2$ as

$$\dot{\hat{b}}_2 \approx -\dot{\sigma} \sin \delta \sin \sigma \sin \gamma \tag{24}$$
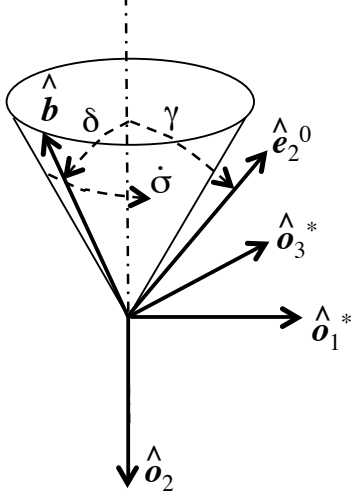
8

Figure 2: Sketch of the geometry for the alignment problem.

Taking into account Eqs. (22), (23), and (24), the control torque $\boldsymbol{M} = -(k_y \dot{\hat{b}}_2)(\hat{\boldsymbol{e}}_2 \times \hat{\boldsymbol{b}})$ can be expressed in terms of component in $\mathbb{F}_O^*$ as

$$\boldsymbol{M} = k_y \dot{\sigma} \begin{pmatrix} -\sin\gamma\cos\gamma\sin^2\delta\sin^2\sigma \\ -\sin^2\gamma\sin^2\delta\sin^2\sigma \\ -\sin^2\gamma\sin\delta\cos\delta\sin\sigma + \sin\gamma\cos\gamma\sin^2\delta\sin\sigma\cos\sigma \end{pmatrix} \tag{25}$$

Provided that the Y-dot control low asymptotically drives the spacecraft towards a pure spin condition around $\hat{\boldsymbol{e}}_2$ on a relatively fast time-scale, maintaining this condition afterwords (see the proof of stability in the previous subsection), any variation $\Delta\boldsymbol{h}$ of the angular momentum $\boldsymbol{h}$ can be interpreted as a rotation of $\hat{\boldsymbol{e}}_2$. The value of $\Delta\boldsymbol{h}$ over one orbit can be obtained by integrating the command torque over one orbital period, that is, it is proportional to the average value of the command torque over two rotations of $\hat{\boldsymbol{b}}$ around the direction $-\hat{\boldsymbol{o}}_2$ in $\mathbb{F}_O^*$, which corresponds to a 4π variation of σ.

From Eq. (25), the first component of $\boldsymbol{M}$, $M_1 \propto -\cos\gamma\sin^2\sigma$ provides a negative increment for the first component of $\Delta\boldsymbol{h}$ in $\mathbb{F}_O$ when $0 < \gamma < \pi/2$, whereas $M_2 \propto -\sin^2\gamma\sin^2\sigma$ always provides a negative increment, independent of the value of γ. Conversely, the third component M_3 of the magnetic control torque has a zero average, at least within the validity of the approximations assumed in this derivation. These considerations allow for inferring the following conclusions:

1. The angular momentum vector remains close to the plane identified by the orbit normal and $\hat{\boldsymbol{e}}_2$ at the initial time t_0, that is, the angle τ is expected to vary on a very slow timescale;

2. The variations of the first and second components of $\boldsymbol{h}$ indicate that the spin axis $\hat{\boldsymbol{e}}_2$ slowly rotates towards the orbit normal, provided that its component along $\hat{\boldsymbol{o}}_2^*$ is constantly reduced, and it is thus expected to achieve increasingly negative values, whereas that along $\hat{\boldsymbol{o}}_1$ increases if $\gamma > \pi/2$, or it decreases when $\gamma < \pi/2$.

Note that in this discussion, the initial direction of the spin axis $\hat{\boldsymbol{e}}_2$ is assumed parallel to that of the angular speed and angular momentum vector at the initial time, where $\boldsymbol{\omega} = \Omega\hat{\boldsymbol{e}}_2$, being Ω the spin rate. When the final spin rate is negative, the spin axis $\hat{\boldsymbol{e}}_2$ will be driven by the Y-dot command law in the opposite direction, asymptotically converging towards an angle $\gamma = \pi$. These conclusions will be validated by the simulations discussed in the next section.

Table 1: Spacecraft data

Parameter	Symbol	Value	Units
Mass distribution			
Maximum moment of inertia	J_{max}	1.60	kg m^2
Intermediate moment of inertia	J_{int}	1.15	kg m^2
Minimum moment of inertia	J_{min}	1.05	kg m^2
Control			
Maximum dipole moment	m_{max}	3.15	A m^2
Reference control gain	k_y	$8.3 \cdot 10^6$	A m^2 s/T

4. Results and Discussion

4.1. Spacecraft response under Y-dot control law

In this section, the validity of the analytical results derived in Section 3, which rely on some simplifying assumptions and approximations, is investigated by means of numerical simulation for a fully nonlinear attitude dynamics model, featuring a tilted dipole model for Earth's magnetic field. The Y-dot control law is implemented as in Eq. (3).

The proof derived in Section 3.2 demonstrates that the Y-dot command law cancels out the initial angular rate of the spacecraft around the x and z axes. If no other command torque is produced, ω_2 asymptotically approaches a value that depends on spacecraft mass distribution (that is, its principal moments of inertia) and initial conditions. There are basically three possibilities, as ω_2 can achieve either a positive, a negative, or zero final value, that is, the spacecraft spins in either direction around its y axis, or it tends to a complete detumbled state. Assuming that the desired spin axis is always the pitch axis y, three scenarios will be considered, where $\hat{e}_2$ is the principal axis of maximum, minimum, or intermediate inertia, respectively. A nano-satellite is considered in the sequel as a test case. Relevant data are summarized in Table 1. Nonetheless, the present analysis is applicable to any rigid spacecraft, provided that the structure of polhodes and separatrices over the inertia ellipsoid depends only on the non-dimensional ratios of inertia moments, $K_1 = (J_2 - J_3)/J_1$ and $K_3 = (J_2 - J_1)/J_3$ [22].

The following simulations are performed by assuming a constant value of the initial angular momentum vector $h_0 = \|\boldsymbol{h}(0)\| = 0.524$ kg m^2/s. Once h_0 is prescribed, the initial kinetic energy $\mathcal{T}_0$ can vary between a maximum and a minimum value, given by $\mathcal{T}_{\mathrm{max}} = h_0^2/(2J_{\mathrm{min}})$ and $\mathcal{T}_{\mathrm{min}} = h_0^2/(2J_{\mathrm{max}})$, respectively. The value $\mathcal{T}_0 = \mathcal{T}_{\mathrm{int}} = h_0^2/(2J_{\mathrm{int}}) = \mathcal{T}^*$ corresponds to the energy level of the separatrices, that divide the surface of the inertia ellipsoid into 4 separate regions of motion [22].

To the purpose of the current analysis, the initial value for the angular velocity components $\boldsymbol{\omega}_0$ is chosen by selecting one point from each one of the polhodes sampled on the surface of the inertia ellipsoid. As the energy variation over the first spin-period is small, due the low available torque, negligible variations of system trajectory in the phase-space would be attained by selecting any other point on the same polhode (i.e., any point with the same initial kinetic energy). For this reason, without loss of generality, the initial angular velocity can be chosen setting at zero the component along the intermediate inertia axis (which is assumed to be $\hat{e}_3$), at least in those cases when the pitch axis itself is not the principal axis of intermediate inertia. The initial values for ω_1 and ω_2 are thus equal to

$$\omega_{1_0} = \omega_1(0) = \pm\sqrt{\frac{h_0^2 - 2J_2\mathcal{T}_0}{J_1\,(J_1 - J_2)}} \;;\;\; \omega_{2_0} = \omega_2(0) = \pm\sqrt{\frac{h_0^2 - 2J_1\mathcal{T}_0}{J_2\,(J_2 - J_1)}} \tag{26}$$

The particular case in which the pitch axis coincides with the intermediate principal axis will be considered at the end of this subsection.

Given these initial conditions, simulations confirm that the Y-dot command law drives the spacecraft towards a pure spin condition around the pitch axis. Figure 3 provides the plot of the asymptotic value
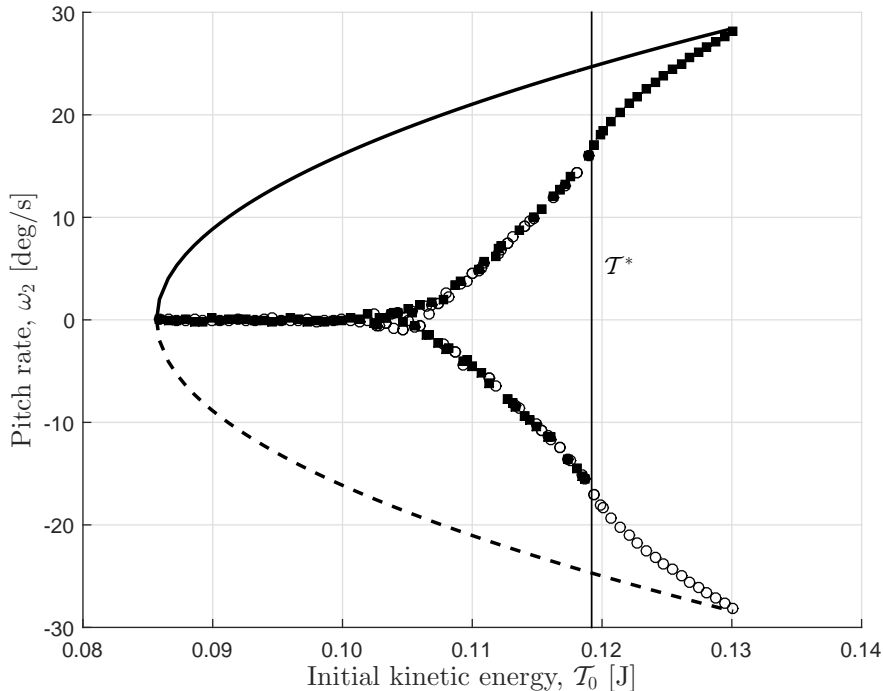
Figure 3: Asymptotic value of ω_2 for $J_2 = J_{\min}$.

of ω_2, when J_2 is the minimum moment of inertia. Solid and dashed lines indicate initial values of ω_2 for positive (counter-clockwise) and negative (clockwise) initial spin rates, respectively. Black squares and white circle markers indicate final values for ω_2 for the positive and negative initial spin rates, respectively. The vertical line identifies the value of kinetic energy $\mathcal{T}^*$ of the separatrices. Again, without loss of generality, the sign for ω_{1_0} is selected concordant with that of ω_{2_0}. In this way, all the energy levels are selected twice, while scanning all of the polhodes on the inertia ellipsoid.

The simulation is stopped when $\omega_1^2 + \omega_3^2 < 0.01^2(\omega_{1_0}^2 + \omega_{3_0}^2)$, that is, when the transverse component of the angular velocity becomes less than 1% of its initial value. In all the considered test cases, the final values of ω_1 and ω_3 are close to zero and they are not reported. Note that for $\mathcal{T}_0 > \mathcal{T}^*$, the asymptotic value of ω_2 maintains the same sign of its initial value. In this sense, the control law transforms the pure spin condition around the axis of minimum inertia into an asymptotically stable equilibrium.

For $\mathcal{T}_0 < \mathcal{T}^*$, three intervals which feature a qualitative different behavior are visible. For values of the initial kinetic energy $\mathcal{T}_0$ less than, but close to $\mathcal{T}^*$, a non zero final value of ω_2 is achieved, where the sign of ω_2 is no longer maintained, and a strong dependency of the sign from the initial value is evident. This is due to the fact that, during the maneuver, the separatrix is crossed somewhere, but the location of the crossing along the evolution of $\boldsymbol{\omega}(t)$ is very sensitive to even minor variations of the initial spin condition. This can inject the spin rate into either one of the regions surrounding the positive and negative pitch spin rates. In this range, no prediction is possible on the direction of the final spinning motion of the spacecraft at the end of the maneuver. For values of $\mathcal{T}_0$ close to the minimum admissible one, $\mathcal{T}_{\min}$, ω_2 converges to zero and the spacecraft is completely detumbled. In an intermediate range, ω_2 does not follow a precise pattern and it can converge to non-zero (yet small) positive or negative values or to zero almost exactly.

As a further comment, the intermediate region becomes smaller as the control gain k_y is decreased. When the nominal value of k_y is used, saturation occurs during most of the pure-spin acquisition portion of the maneuver. In this condition, also a relatively small error signal causes the torque-rod to produce the maximum dipole moment and the behavior of the control law resembles that of a switching logic based on the sign of the error signal. Chattering phenomena can occur with rapid changes in the sign of the control
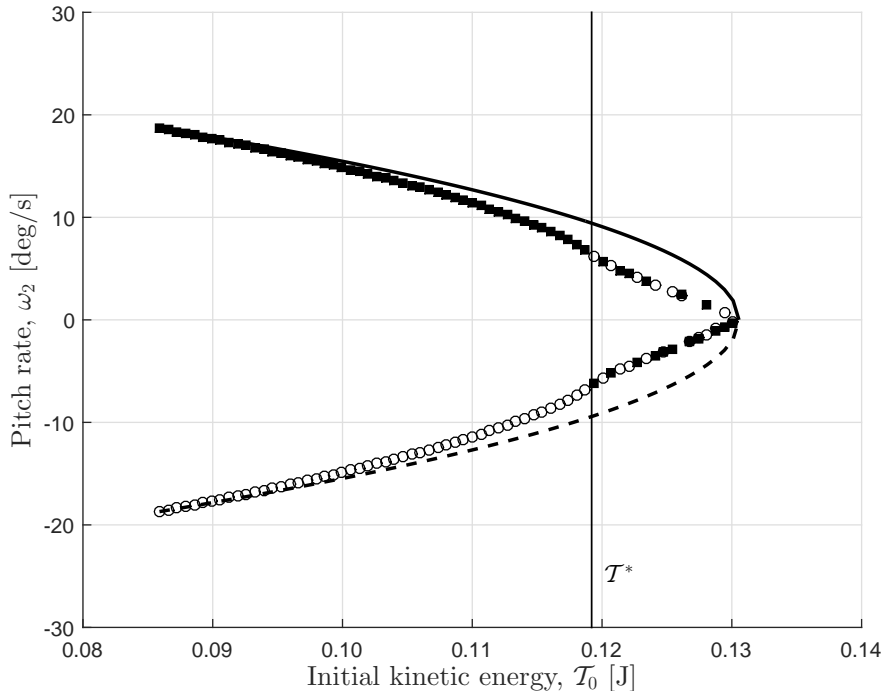
Figure 4: Asymptotic value of ω_2 for $J_2 = J_{\mathrm{max}}$.

torque, which in turn cause the dispersion in the values of steady-state pitch rates observed in Fig. 3. When k_y is reduced by a factor 20 or higher, saturation of the torque-rods occurs only at the very beginning of the maneuver. During the final phase convergence towards a pure spin condition is smoother and the resulting plot of the final states for ω_2 shows a more regular pattern.

When $\hat{e}_2$ is the principal axis of maximum inertia a similar pattern is obtained (Fig. 4), with two major differences: (i) the region of complete detumbling is reduced to one point, for $\mathcal{T}_0 = \mathcal{T}_{\mathrm{max}}$, and (ii) the behavior of the final spin rate in the region where crossing of the separatrix occurs appears more regular. This means that, for $\mathcal{T}_0 < \mathcal{T}^*$, a pure spin condition around the y axis is achieved which preserves the sign of the initial value of ω_2, whereas for $\mathcal{T}_0 > \mathcal{T}^*$, the motion starts outside of the regions surrounding the pure spin around y, and the sign of ω_2 depends on where the crossing of the separatrix takes place.

Finally, when $\hat{e}_2$ is the principal axis of intermediate inertia, the initial angular velocity is chosen such that the component along the intermediate inertia axis is zero, that is $\omega_{2_0} = 0$, whereas ω_{1_0} and ω_{3_0} are defined as ω_{2_0} and ω_{1_0} in Eq. (26), respectively. However, in this scenario, all the angular velocity components converge to zero, no matter what the initial conditions are. This means that the Y-dot control law provides a means for complete detumbling of the spacecraft, independently of the initial spin condition, when J_2 is the intermediate principal moment of inertia.

A total of eight different solutions is thus present, as summarized in Table 2, where each solution type is labeled with a letter from A to H depending on the value of J_2 and the asymptotic value achieved by ω_2.

These results represent a relevant piece of information from the practical standpoint, inasmuch as complete detumbling can be obtained by use of only one single magnetic torque-rod, provided that its dipole moment is aligned with the intermediate axis of inertia. Conversely, when the spacecraft is expected to spin around the y axis in one prescribed direction (regardless of the initial angular rate), the Y-dot control law does not guarantee that the desired direction of spin will be acquired when the initial spin rate is unknown. This is a common condition for nanosatellites, that are launched as secondary payloads and may be injected into their orbit with a tumbling motion, with an angular rate that may vary over a wide range around all three axis. In this case, at least one additional torque-rod is required to modulate the asymptotic value of

12

Table 2: Classification of solutions

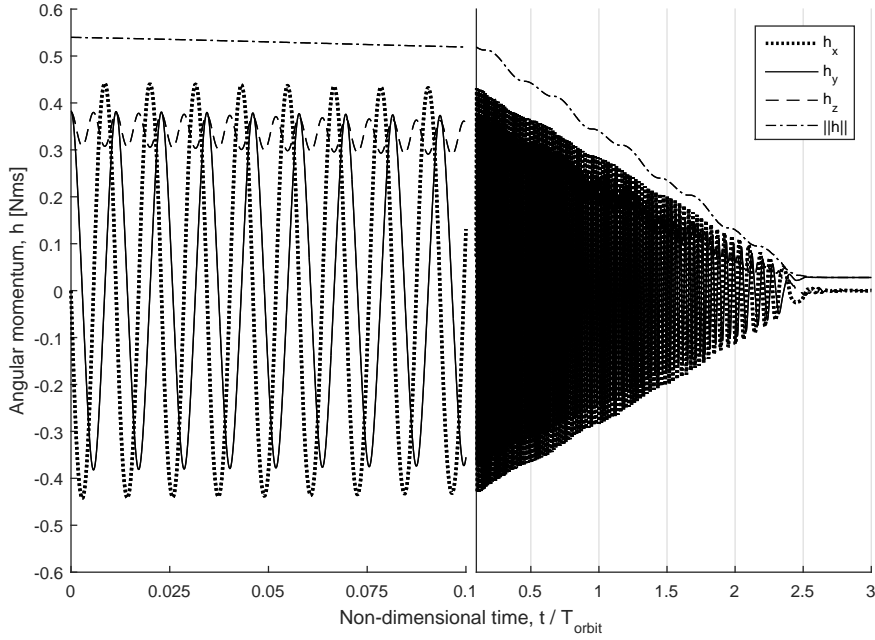| Type	Initial kinetic energy	Asymptotic value of ω_2	
$J_2 = J_{\min}$			
A	$\mathcal{T}^* < \mathcal{T}_0 < \mathcal{T}_{\max}$	$\omega_2 \to \omega_{2_F}$,	$\omega_{2_0} \cdot \omega_{2_F} > 0$
B	$\mathcal{T}_{\min} < \mathcal{T}_0 < \mathcal{T}^*$	$\omega_2 \to \omega_{2_F}$,	$\omega_{2_0} \cdot \omega_{2_F} > 0$
C	$\mathcal{T}_{\min} < \mathcal{T}_0 < \mathcal{T}^*$	$\omega_2 \to \omega_{2_F}$,	$\omega_{2_0} \cdot \omega_{2_F} < 0$
D	$\mathcal{T}_{\min} < \mathcal{T}_0 < \mathcal{T}^*$	$\omega_2 \to 0$	
$J_2 = J_{\max}$			
E	$\mathcal{T}_{\min} < \mathcal{T}_0 < \mathcal{T}^*$	$\omega_2 \to \omega_{2_F}$,	$\omega_{2_0} \cdot \omega_{2_F} > 0$
F	$\mathcal{T}^* < \mathcal{T}_0 < \mathcal{T}_{\max}$	$\omega_2 \to \omega_{2_F}$,	$\omega_{2_0} \cdot \omega_{2_F} > 0$
G	$\mathcal{T}^* < \mathcal{T}_0 < \mathcal{T}_{\max}$	$\omega_2 \to \omega_{2_F}$,	$\omega_{2_0} \cdot \omega_{2_F} < 0$
$J_2 = J_{\mathrm{int}}$			
H	$\mathcal{T}_{\min} < \mathcal{T}_0 < \mathcal{T}_{\max}$	$\omega_2 \to 0$	

ω_2, as discussed in [9].

Figure 5: Time-histories of the components and norm of the angular momentum vector during a type B spin acquisition maneuver.

As an example, the time-history of the components of the angular momentum vector for a spin acquisition maneuver of type B is reported in Fig. 5, when the desired spin axis is the principal axis of minimum inertia (that is, $J_2 = J_{\min}$). The plot clearly shows how the component of the angular momentum vector along the pitch axis asymptotically approaches a non-zero positive value, whereas h_1 and h_3 converge to 0, thus proving that a pure spin condition around the y axis is achieved.

The same solution is shown in Fig. 6.a in terms of body frame components of the angular velocity vector, plotted over the inertia ellipsoid. Figure 6.b provides the same representation for a type F solution, with $J_2 = J_{\max}$. Provided that the norm of the angular momentum vector $\|\boldsymbol{h}\|$ is not constant during the maneuver (dash-dot line in Fig. 5), the ellipsoid is scaled with respect to the current value of the angular momentum vector and a normalized angular velocity vector is introduced, $\boldsymbol{\omega}^\star = \boldsymbol{J}^{-1}(\boldsymbol{h}/\|\boldsymbol{h}\|)$. The final spin
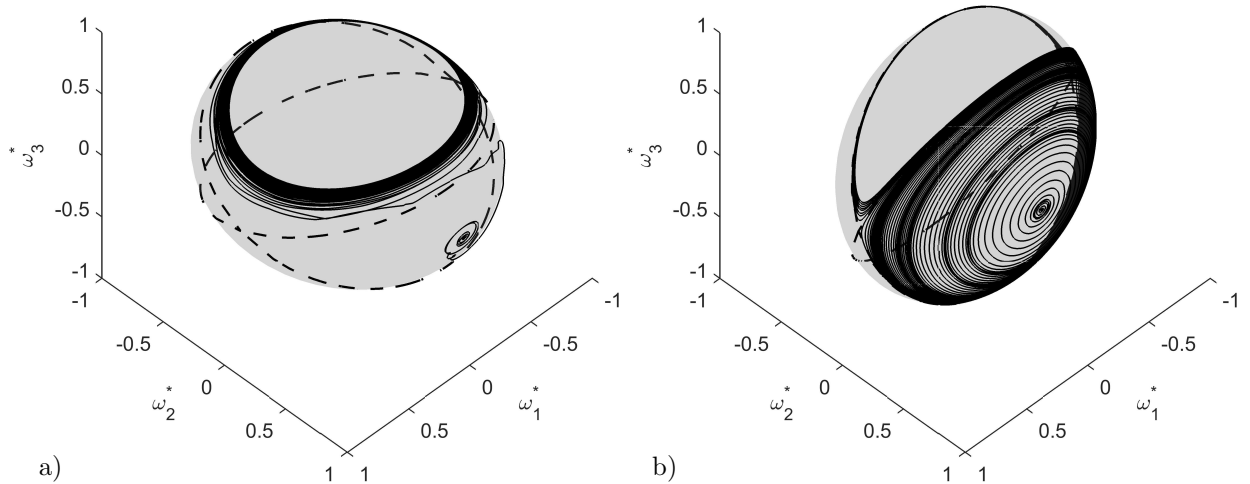
Figure 6: Body frame components of the angular velocity vector over the scaled inertia ellipsoid showing crossing of the separatrix for a type B (a) and a type F (b) maneuver.

rate depends on the sign of ω_2 when crossing of the separatrix occurs. A variation of the initial condition (even a small one, in some cases) can cause the crossing to occur along a different separatrix, thus driving the angular rate on the opposite side of the ellipsoid, and making the spin condition converge towards a final pitch spin rate with a different sign.

Note that the representation of Fig. 6 does not suit those cases where complete detumbling is achieved (*i.e.* types D and H solutions) as the norm of the angular momentum vector asymptotically approaches zero, and the inertia ellipsoid degenerates to a point. Nevertheless, the evolution of $\boldsymbol{\omega}^\star$ on the normalized inertia ellipsoid provides useful information on the final spin condition when a non-zero spin rate is achieved.

4.2. Alignment of spin axis with normal to the orbit plane

In this subsection, the alignment of spin axis $\hat{\boldsymbol{e}}_2$ with the direction of the orbit normal $\hat{\boldsymbol{o}}_2$, which was proven in Section 3.3 by evaluating an approximation of the average control torque for the Y-dot command law over one orbit, is confirmed on the basis of a thorough set of numerical simulations. In this respect, Fig. 7 provides the evolution of the angle between the spin axis and the orbit normal, $\gamma = \cos^{-1}(\hat{\boldsymbol{o}}_2 \cdot \hat{\boldsymbol{e}}_2)$ for a type F spin acquisition maneuver.

First of all, one notes that alignment of the spin axis towards the orbit normal requires a relatively long time. For the considered values of initial angular momentum h_0, dipole saturation level $m_{\max}$, and control law gain k_y, the pure spin condition is obtained in less than one orbit period, whereas several orbits are necessary for completing the required alignment within $1°$ of accuracy (about 5 orbits, for the particular test case represented in Fig. 7).

As in the case of convergence of $\boldsymbol{h}$ towards a pure spin condition in the body frame, also convergence of $\boldsymbol{h} = J_2 \omega_{2_f} \hat{\boldsymbol{e}}_2$ towards the opposite to the orbit normal, as seen in the orbit frame, may follow different paths, depending on the initial conditions. Figures 8.a and 8.b show the position of the projection of the spin axis $\hat{\boldsymbol{e}}_2$ on the orbit plane for the two cases of type B and F considered above. It is clear that, for case B, a rather disordered tumbling motion is maintained during the initial phase, until a slow but almost monotonic convergence to the final spin state is achieved. Conversely, case F shows a more regular behavior during the initial phase. After crossing of the separatrix, several precession revolutions around the orbit normal are necessary for driving the spin axis onto the orbit normal.

4.3. Analysis of the control gain

The behavior discussed in the previous subsection depends on several factors, some of which cannot be determined *a priori*, such as the initial condition of the tumbling motion. Others, such as maximum magnetic
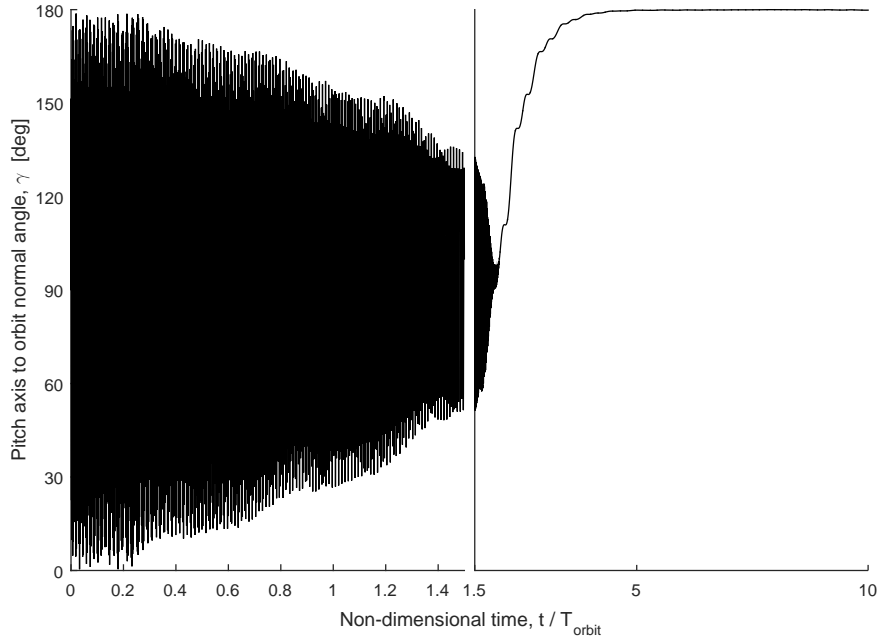
14

Figure 7: Evolution of the angular distance between pitch axis and orbit normal, γ, over two time-scales for fast rotation $(0 - 1.5)$ and slow convergence $(1.5 - 10)$ respectively.
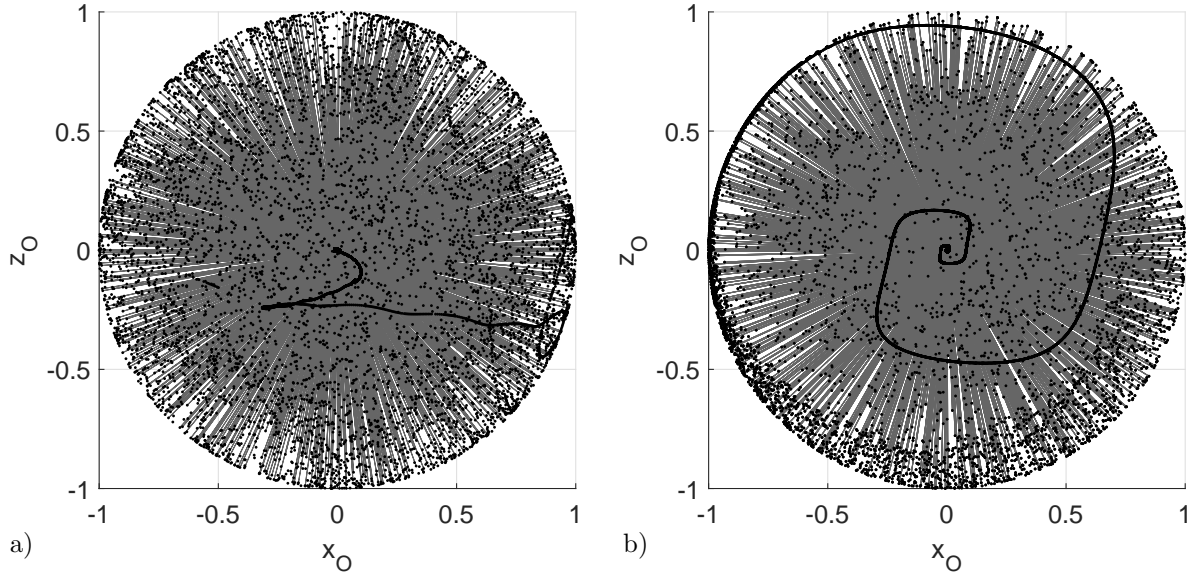

Figure 8: Projection of $\hat{e}_2$ on the orbit plane during convergence to the orbit normal $\hat{o}_2$.

dipole moment and control law gain, are specified during the design phase. It is clear that a stronger dipole moment allows for a faster maneuver, inasmuch as the torque-rod delivers a higher control torque during the initial phase of the maneuver, when the angular momentum is reduced by means of dissipation of kinetic energy.

Conversely, the choice of the control gain may not be straightforward when magnetic actuators are employed. As an example, in some application [7, 5], there exists an optimal value for the control law gain between the two extreme cases, inasmuch as a weak control gain determines a slow convergence, but an
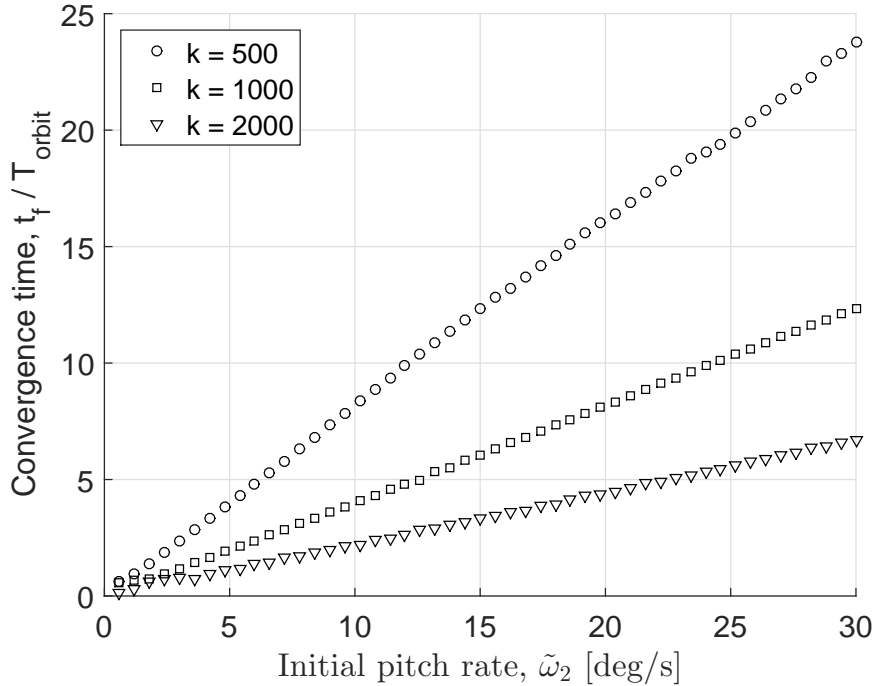
15

Figure 9: Spin axis convergence to the orbit normal: time required as a function of spin rate and control gain factor.

excessively high value determines a rapid cancellation of two components of the angular velocity, followed by a slow convergence towards the desired state, with the angular momentum vector almost aligned with the magnetic field. For this reason, a parametric analysis was performed to better understand the effect of the control gain $k_y = k \left(M_\oplus / r_c^3 \right)^{-1}$ on the time required for convergence to the final spin state around a spin axis parallel to the orbit normal.

All the simulations start from the same initial attitude, such that the desired spin axis $\hat{e}_2$ is initially perpendicular to $\hat{o}_2$ (i.e., the spin axis is tilted 90 deg away from its expected final condition). The initial angular speed is set equal to $\boldsymbol{\omega} = \tilde{\omega}_2 \hat{e}_2$. This is consistent with results reported above, where convergence towards a pure spin condition about the commanded axis is faster than convergence of the spin axis during the orbit normal. During this initial phase, the effect of the control gain on the structure of solutions is minimal. Plots like those reported in Figs. 3 and 4 do not change significantly as k_y is varied by two orders of magnitude. The only minor effect is that, as the control gain is reduced, convergence is smoother and the curves representing the asymptotic values of ω_2 become more regular.

In what follows, it will be assumed that the acquisition of the pure spin condition is completed during a previous maneuver phase. Results in terms of number of orbits necessary for taking the spin axis within 1 deg from the normal to the orbit plane are provided for a reasonably wide range of initial spin rates, $\tilde{\omega}_2$, and different values of the control gain factor k.

Figure 9 shows that the time required to reach convergence to the orbit normal (within 1 deg of accuracy) depends almost linearly on both the initial angular rate, $\tilde{\omega}_{2_0}$, for a given control gain, and the inverse of the control gain k_y. When the Y-dot control law is adopted, the behavior of the closed-loop system is thus intuitive, where higher gains result into a faster convergence, with no exceptions. For high values of k_y, the behavior resembles that of a switching logic based on the sign of the error signal, rather than a proportional command, for most of the maneuver time. Moreover, there is one practical issue that needs to be carefully accounted for, that is, higher gains also result into higher energy consumption, inasmuch as the magneto-torquer works at saturation for a longer time. In this respect, the tradeoff between convergence time and electrical power expenditure needs to be carefully addressed.

5. Conclusions

An analytical proof of global asymptotic stability towards a pure spin condition was derived for the Y-dot control law, assuming that the control dipole moment is proportional to the time derivative of the component of the geomagnetic field along the direction of the spin axis. After acquisition of the pure spin condition, the spin axis is driven towards the orbit normal. This phenomenon was explained by evaluating the average magnetic control torque over one orbit, proving that, regardless of the initial attitude, the magnetic torque reduces the angle between the direction of the angular momentum vector of the spacecraft and the orbital angular velocity.

Numerical simulations demonstrate the validity of the analytical results, while highlighting interesting features in the behavior of the spacecraft under the action of the Y-dot command law. In particular, the final spin condition depends on the initial tumbling motion, but it can be hardly predictable, when crossing of one separatrix occurs during the despin. In some cases, the Y-dot command law drives the spacecraft towards a de-spun condition. This is always the case when the pitch axis is the principal axis of intermediate inertia. The effect of control gain on convergence time was also quantified, proving that an increase in control gain reduces converge time for both maneuver phases (that is, acquisition of a pure spin state and alignment of the spin axis to the orbit normal) at the cost of an increased dispersion of the final state, due to the effects of saturation on the initial part of the maneuver.

References

[1] M. Lovera, A. Astolfi, Spacecraft attitude control using magnetic actuators, Automatica 40 (8) (2004) 1405–1414.

[2] Y. J. Cheon, S. H. Lee, J. H. Kim, Fully magnetic devices-based control for gyroless target pointing of a spinning spacecraft, Aerospace and Electronic Systems, IEEE Transactions on 46 (3) (2010) 1484–1491.

[3] H. B. Hablani, Comparative stability analysis and performance of magnetic controllers for bias momentum satellites, Journal of Guidance, Control, and Dynamics 18 (6) (1995) 1313–1320.

[4] A. C. Stickler, K. Alfriend, Elementary magnetic attitude control system, Journal of Spacecraft and Rockets 13 (5) (1976) 282–287.

[5] G. Avanzini, F. Giulietti, Magnetic detumbling of a rigid spacecraft, Journal of Guidance, Control, and Dynamics 35 (4) (2012) 1326–1334.

[6] T. Flatley, W. Morgenstern, A. Reth, F. Bauer, A B-Dot Acquisition Controller for the RADARSAT Spacecraft, in: Flight Mechanics Symposium, edited by D. M. Walls, NASA Goddard Space Flight Center, Greenbelt, MD, May 1997, 79–89, 1997.

[7] G. Avanzini, E. L. de Angelis, F. Giulietti, Acquisition of a Desired Pure-Spin Condition for a Magnetically Actuated Spacecraft, Journal of Guidance, Control, and Dynamics 36 (6) (2013) 1816–1821.

[8] H. Steyn, Y. Hashida, V. Lappas, An Attitude Control System and Commissioning Results of the SNAP-1 Nanosatellite, in: Proceedings of the 14th AIAA/USU Conference on Small Satellites, SSC00-VIII-8, Logan, UT, 2000.

[9] A. Anderson, J. Sellers, Y. Hashida, Attitude determination and control system simulation and analysis for low-cost micro-satellites, in: Aerospace Conference, 2004. Proceedings. 2004 IEEE, vol. 5, ISSN 1095-323X, 29–34 Vol.5, doi: 10.1109/AERO.2004.1368099, 2004.

[10] W. Steyn, Y. Hashida, In-orbit attitude and orbit control commissioning of UoSAT-12, in: Spacecraft Guidance, Navigation and Control Systems, vol. 425, 95, 2000.

[11] A. S. Mohammed, An attitude determination and control system of the Alsat-1 first Algerian microsatellite, in: Recent Advances in Space Technologies, 2003. RAST'03. International Conference on. Proceedings of, IEEE, 171–176, 2003.

[12] W. Steyn, An Attitude Control System for SumbandilaSAT an Earth Observation Satellite, in: ESA Special Publication, vol. 660, 83, 2008.

[13] M. Ovchinnikov, D. Roldugin, V. Penkov, Asymptotic study of a complete magnetic attitude control cycle providing a single-axis orientation, Acta Astronautica 77 (0) (2012) 48 – 60, ISSN 0094-5765.

[14] J. R. Wertz, Spacecraft Attitude Determination and Control, Springer, 1978.

[15] D. Roldugin, P. Testani, Spin-stabilized satellite magnetic attitude control scheme without initial detumbling, Acta Astronautica 94 (1) (2014) 446 – 454, ISSN 0094-5765, doi:http://dx.doi.org/10.1016/j.actaastro.2013.01.011.

[16] A. Slawinskia, On the comparative analysis of some criteria of stability of motion, International Journal of Non-Linear Mechanics 33 (5) (1998) 783 – 799, ISSN 0020-7462, doi:http://dx.doi.org/10.1016/S0020-7462(97)00051-6.

[17] S. K. Choi, K. S. Koo, K. H. Lee, Lipschitz stability and exponential asymptotic stability in perturbed systems, J. Korean Math. Soc 29 (1) (1992) 175–190.

[18] B. Wie, Space vehicle dynamics and control, Aiaa, 1998.

[19] F. M. Dannan, S. Elaydi, Lipschitz stability of nonlinear systems of differential equations. II. Liapunov functions, Journal of Mathematical Analysis and Applications 143 (2) (1989) 517 – 529, ISSN 0022-247X, doi:http://dx.doi.org/10.1016/0022-247X(89)90057-7.

[20] Z. S. Athanassov, Perturbation theorems for nonlinear systems of ordinary differential equations, Journal of Mathematical Analysis and Applications 86 (1) (1982) 194–207.

[21] H. K. Khalil, J. Grizzle, Nonlinear systems, Prentice Hall, 2002.

[22] P. C. Hughes, Spacecraft Attitude Dynamics, Dover, 2004.